Research Paper

Journal of Engineering and Technological Sciences

Modelling of Sulfur Dioxide Removal by Seawater in a Flue Gas Desulfurization Absorber

Kania Dewi[1], Anders Andreasen[2] & Addina Shafiyya Ediansjah[1]

[1]Study Program of Environmental Engineering, Faculty of Civil and Environmental Engineering, Air and Waste Research Group, Institut Teknologi Bandung, Jalan Ganesa No 10, Bandung 40132, Indonesia
[2] Ramboll Energy, Energy Transition, Process Department, Bavnehøjvej 5, Esbjerg, Denmark

*Corresponding author: kaniadewi@itb.ac.id

Abstract

Although Indonesia has set a target for increasing the use of renewable energy for electricity generation, the use of coal as a source of energy will still dominate at least until 2040. Sulfur dioxide (SO_2) along with other gases and particulates released from the use of coal in coal-fired power plants (CFPPs) may cause air pollution. The use of seawater, an abundant source of absorbent in a maritime country such as Indonesia, in flue gas desulfurization (SWFGD) absorbers, is an economical option for treating SO_2 in an absorption tower compared to other alkaline chemicals, e.g. limestone ($CaCO_3$) or magnesium hydroxide ($Mg(OH)_2$). A model, which correlates the equilibrium of the reaction with the salinity of the absorbent, was developed to predict the sulfur dioxide scrubbing process inside an SWFGD absorber. The simulation also took into account the mass and energy balance during the scrubbing process. The calibration using field SWFGD data showed a good correspondence between field data and modelling results.

Keywords: *absorber; flue gas desulfurization; modelling; seawater; sulfur dioxide.*

Introduction

Wet flue gas desulfurization (WFGD) absorbers are commonly used to remove SO_2 emitted from CFPPs. Limestone is widely applied as an absorbent, since it is simple, cheap and was the most developed SO_2 wet removal process available from the early 1980s until the 1990s. However, the use of limestone still carries some inherent challenges such as mining source availability, transportation to the CFPP site as well as byproducts (gypsum) management. Although gypsum has an economic value, it is classified as a hazardous material in Indonesia according to the Government of Indonesia Regulation No. 101/2014 concerning Waste Management of Hazardous and Toxic Materials. Thus, gypsum from WFGD absorber byproducts must be handled as a hazardous material, which eventually leads to an increase of the operational cost of CFPPs.

Based on data from three major international SWFGD vendors, SWFGD processes have been used since 1995 but gained attention and popularity from 2010. At least two seaside CFPPs in Indonesia applied this system in 2019. There are two main advantages of utilizing seawater as absorbent, i.e., the abundant availability of absorbent, especially in a maritime country such as Indonesia, and simple effluent handling due to the absence of unwanted byproducts [1]. The salinity of seawater used is highly dependent on the region and the conditions of the waters under consideration, but the cation and anion constituents contained in the water are approximately the same. Alkali compounds generally present in seawater are HCO_3^-, CO_3^{2-}, OH^-, HPO_4^{2-} and other trace elements. The main contributor to the alkalinity of seawater is HCO_3- [1], and the common seawater salinity is 35 ppt (g/kg) [2]. Table 1 summarizes the differences between a WFGD and an SWFGD.

ISSN: 2337-5779

J. Eng. Technol. Sci. Vol. 56, No. 4, 2024, 510-520
DOI: 10.5614/j.eng.technol.sci.2024.56.4.7

DOI: 10.5614/j.eng.technol.sci.2024.56.4.7

Table 1 Differences in SO_2 removal efficiency, pH and generated byproduct of a WFGD and an SWFGD absorber.

Parameter	WFGD	SWFGD	Source
SO_2 removal efficiency	80 – 95%	90 – 98%	[3]
	95 – 99%	90 – 95%	[4]
pH			
– Inlet		8.0 – 8.2	[3]
– Outlet	4.73 – 6.59	3.0 – 4.0	[5,3]
Generated byproduct	Large amount of gypsum	-	[3]
Effluent characteristics	Increased suspended solids	Slight increase of SO_4^{2-}	[3]

After being used as an absorbent in removing SO_2 gas in an SWFGD absorber, the seawater pH in the SWFGD absorber effluent will decrease due to the increase of acid species. Therefore, it must be treated using aeration before being released back to the sea and mixed with additional seawater from the condenser. During aeration, large amounts of oxygen (O_2) gas will be injected to remove dissolved CO_2 in the water [6] and oxidize SO_3^{2-} to SO_4^{2-} to reduce chemical oxygen demand (COD) [3].

A numerical study that modelled the interface between seawater and SO_2 gas in a single droplet of seawater for maritime engines has shown that seawater can be used as a promising absorbent compared to conventional ones such as NaOH, limestone, and NaCl [1]. Another numerical study was carried out in a maritime engine, considering salinity as the limiting factor in the chemical reaction [2]. Similar numerical modelling, which correlated the equilibrium constant of the absorption process and the removal efficiency of SO_2 within a packed tower, was done previously [7].

The present study combined the numerical model results given by [7] and [2] as well as other modelling information from [3, 6, 8, 9, 10-17], which was then used to evaluate the applicability of seawater in a flue gas desulfurization process in Indonesia.

Methodology

A model was set up based on the reaction balance, mass balance, and energy balance of SO_2 absorption within an SWFGD absorber. Results of the calculations are presented in the form of SO_2 concentration and temperature along the SWFGD absorber. A typical system of an SWFGD absorber (a packed tower type) is illustrated in Figure 1. The changes in concentration or mole faction of the SO_2 in the gas stream along the height of the absorption tower are illustrated in Figure 2.

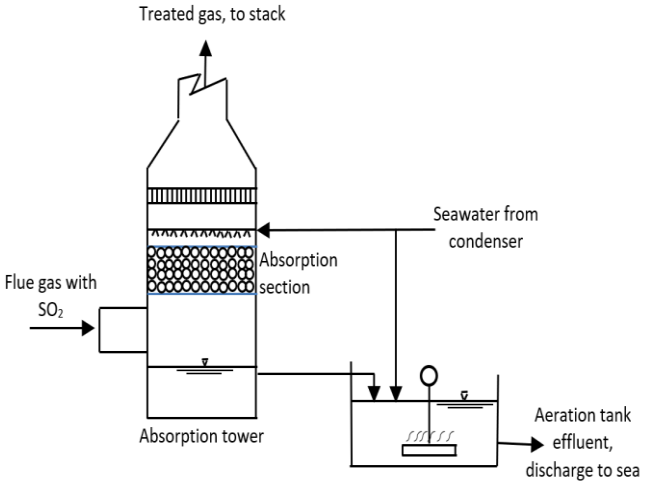

Figure 1 An SWFGD system with an aeration tank.

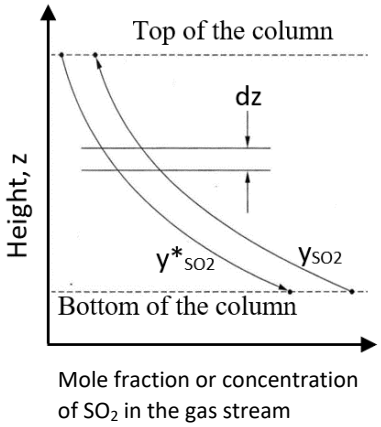

Figure 2 Simplified schematic diagram of the changes in SO_2 mole fraction in the absorption tower [18].

The absorption tower operates in a counterflow configuration with liquid flowing down the column by gravity and the gas flowing up the column driven by the decrease in pressure from bottom to top. The curve in Figure 2 shows that the mole fraction of SO_2 (y_{SO2}), the gas to be absorbed, decreases from its high value where it enters the bottom of the absorption tower to its low value at the outlet of the absorption tower. The curve also shows the mole fraction of SO_2 (y^*_{SO2}) that would be in equilibrium with the liquid absorbent, its value increasing from the top of the column to the bottom of the column, as absorbent removes the SO_2 from the gas stream.

Model Assumptions

The SO_2 absorption model in seawater absorbent used in this study is a non-isothermal model considering chemical reactions in the gas and liquid phases. The mass balance, the coefficient of heat transfer resistance in the gas and liquid phases and the evaporation of the liquid form the basis for the preparation of mathematical models. The model was developed for the steady state adiabatic operating conditions with fluctuations in gas and liquid discharge due to evaporation with resistance due to heat transfer not being taken into account.

Henry's Law and Dissociation-Neutralization Reaction

The following sequence of chemical reactions shows the absorption of SO_2 from gas phase to liquid phase in Eq. (1), bisulfite $HSO_3^-(aq)$ in Eq. (2), dissociation reaction of bisulfite to sulfite $SO_3^{2-}(aq)$ in Eq. (3), neutralization of $H_3O^+(aq)$ that has been formed by the seawater in Eq. (4), dissociation reaction of hydrogen sulfate to sulfate present in the seawater in Eq. (5), absorption of CO_2 gas in water in Eq. (6), the dissociation of water into H^+ and OH- in Eq. (7).

$$SO_2(g) \leftrightarrow SO_2(aq) \quad (1)$$

$$SO_2(aq) + 2H_2O(l) \leftrightarrow HSO_3^-(aq) + H_3O^+(aq) \quad (2)$$

$$HSO_3^-(aq) + H_2O(l) \leftrightarrow SO_3^{2-}(aq) + H_3O^+(aq) \quad (3)$$

$$HCO_3^-(aq) + H_3O^+(aq) \leftrightarrow CO_2(aq) + 2H_2O(l) \quad (4)$$

$$HSO_4^-(aq) + H_2O(l) \leftrightarrow SO_4^{2-}(aq) + H_3O^+(aq) \quad (5)$$

$$CO_2(aq) \leftrightarrow CO_2(g) \quad (6)$$

$$H_2O \leftrightarrow H^+ + OH^- \quad (7)$$

The dissolution reaction of SO_2 in the gas phase into the water phase occurs in a thin film layer that separates the gas and water according to Henry's law in Eq. (8):

$$[SO_2(aq)] = p_{SO_2} k_H \quad (8)$$

Where pSO_2 is the partial pressure of SO_2, $[SO_2(aq)]$ is the concentration of SO_2 in the solution and k_H is Henry's constant expressed by Eq. (9):

$$k_H = k°_H e^{\frac{-\Delta H_{soln}}{R}(\frac{1}{T}-\frac{1}{T°})} \quad (9)$$

DOI: 10.5614/j.eng.technol.sci.2024.56.4.7

Where $k°_H$ is Henry's constant under reference conditions, ΔH_{soln} is the enthalpy of the solution, T is the temperature and T° is the temperature at the reference condition (298.15 K). By entering Henry's constant obtained from experiment [15], a value for $k_H°$ value of 1.2 mole/(kg atm) was derived with a slope ($-\Delta H_{soln}/R$) of 2850 K. This was in accordance with the data listed in [19]. Calculation of chemical compound changes in the system is a function of the temperature-dependent dissociation coefficient. The dissociation coefficient developed in [10] has a limited seawater temperature range of 278.15 to 318.15 K. In this case, the dissociation coefficient calibration was applied based on temperature differences [20]. Dissociation coefficient calibration is shown in Eq. (10).

$$ln\frac{K_{(T_2)}}{K_{(T_1)}} = \frac{-\Delta H^{\circ}}{R}\left(\frac{T_1 - T_2}{T_1 T_2}\right) \tag{10}$$

The dissolution and neutralization processes in reaction 2 to 5 can be expressed by Eqs. (11) to (14):

$$K_{II} = \frac{[HSO_3^-][H_3O^+]}{[SO_2(aq)]} \tag{11}$$

$$K_{III} = \frac{[SO_3^{2-}][H_3O^+]}{[HSO_3^-]} \tag{12}$$

$$K_{IV} = \frac{[CO_2(aq)]}{[HCO_3^-][H_3O^+]} = K_a^{-1} \tag{13}$$

$$K_V = \frac{[SO_4^{2-}][H_3O^+]}{[HSO_4^-]} \tag{14}$$

Salinity is another factor that has an influence on the constant K_a. The empirical correlation between temperature and salinity is described in Eq. [11], where S is the salinity and A, B, C, D, and E are coefficients that depend on temperature as expressed in Eqs. (15) and (16):

$$\ln K_a = A + BS^{0,5} + CS + DS^{1,5} + ES^2 \tag{15}$$

$$\text{Ln } K_* = 2{,}83655 - \frac{2307{,}1266}{T} - 1{,}4429413 \ln T + \left(-0{,}20760841 - \frac{4{,}0484}{T}\right) S^{0,5} + 0{,}08468345S - 0{,}00654208S^1 \tag{16}$$

Mass Balance

Mass balance and energy balance equations were derived from [7]. The size of the WFGD can be determined by applying the principle of mass transfer as in Eq. (17):

$$ln\frac{y_{out}}{y_{in}} = K_g a \frac{P}{G^1} \tag{17}$$

Where y_{in} is the SO_2 concentration at the inlet (ppm), y_{out} is the SO_2 concentration at the outlet, K_g is the overall mass transfer coefficient (kg mole/m^2 hour atm), P is the pressure (atm), a is the gas-liquid contact area (m^2 /m^3), and G^1 is the molear mass velocity of the gas (kg mole/m^2 hr).

The global mass transfer coefficient can be determined using Eq. (18):

$$\frac{1}{K_g} = \frac{1}{k_g} + \frac{H}{\emptyset k_L} \tag{18}$$

where k_g is the mass transfer coefficient of the gas phase (kg mole/ m^2 hour atm), k_L is the mass transfer coefficient of the liquid phase (m/hour), H is Henry's constant for SO_2 (atm hour/kg mole), and Φ is the enhancement factor. The values of k_g and k_L were taken for packed towers of the Raschig rings type [17].

The variation of SO_2 concentration in the gas phase along the absorber can be described by Eq. (19):

$$\frac{dy_{SO_2}}{dz} = -\frac{N_{SO_2} a a M_a}{Q_g \rho_g} \tag{19}$$

with the mass transfer flux (N_{SO2}) derived from Eq. (20):

$$N_{SO_2} = K_{gs}(y_{SO_2} - y_{SO_{2i}}) \tag{20}$$

In the above equation, y_{SO2i} is the equilibrium concentration of SO_2 in the gas phase, and K_{gs} is the overall mass transfer coefficient of SO_2, which is calculated based on the mass transfer coefficients of the gas and liquid phases.

The calculation of the SO_2 fraction (y_{SO2i}) at equilibrium condition is estimated using Eqs. (21) and (22):

$$\{H^+\} = \frac{10^{-pH}}{\gamma_{H+}} + [HSO_3^-] + 2[SO_3^{2-}] - [H_2CO_3^*]_g - [HSO_4^-] \quad (21)$$

where $[H_2CO_3^*]_g$ represents the H_2CO_3 and $CO_{2(aq)}$ species during the SO_2 absorption process with $[H_2CO_3^*]_g = [H_2CO_3^*]_i - [H_2CO_3^*]_f$. The subscripts *g*, *i* and *f* refer to the gas, interface, and fluid in respective order. As a simplification, the value of $[H_2CO_3]_f = CO_{2(aq)}$ because it is dominated by $CO_{2(aq)}$ species. The concentration of $[H_2CO_3]_i$ in water is the HCO_{3-} species produced by the reaction of $CO_{2(aq)}$ with water [9]. The initial alkalinity of seawater, which is 2400 mole/kg H_2O, is also added as initial condition.

$$y_{SO_{2i(aq)}} = \frac{T_{SO_2} x H_{SO_2}}{P}\left[\frac{1}{\gamma_{SO_2}} + \frac{K_{II}}{\{H^+\} x \gamma_{HSO_3}} + \frac{K_{II} x K_{III}}{\{H^+\}^2 x \gamma_{SO_3}}\right]^{-1} \quad (22)$$

For every variation of SO_2 concentration along the absorber, there is an equilibrium in both phases as a function of temperature, partial pressure of SO_2 in the gas phase, and the composition of seawater. The variation of water vapor in the gas phase along the absorber is described by Eq. (23):

$$\frac{dy_w}{dz} = \frac{N_w A a M_a}{Q_g \rho_g} \quad (23)$$

with the mass transfer flux described by the notation N_w as in Eq. (24):

$$N_w = k_{gw}(y_{wi} - y_w) \quad (24)$$

The concentration of SO_2 gas passing through the gas layer will be absorbed in the liquid according to the Two-Film Theory law with the mass balance equation for the SO_2 gas concentration in the liquid phase (X_d) along absorber described by Eq. (25):

$$\frac{dX_d}{dz} = -\frac{N_{SO_2} A a M_w}{Q_l \rho_l} \quad (25)$$

Energy Balance

The transfer of water vapor from the liquid layer to the gas layer occurs due to the simultaneous transfer of mass and energy. The variation in temperature (energy balance) of the gas phase along the absorber is described by Eq. (26):

$$\frac{dT_g}{dz} = -\frac{haA(T_g - T_l)}{Q_g \rho_g (C_{pg} + y_w C_{pv})} \quad (26)$$

The liquid temperature depends on the convection coefficient of the gas, the evaporation of the liquid, and the heat generated from the reaction. The variation in temperature (energy balance) of the liquid phase along a point in the absorber is described by Eq. (27):

$$\frac{dT_l}{dz} = -\frac{N_w a A M_w \gamma + haA(T_g - T_l) + \Delta H_r N_{SO_2} M_{SO_2}}{Q_l \rho_l C_{pl}} \quad (27)$$

Solution of Numerical Model

Figure 3 illustrates the schematic of numerical model solution. G_{in} and G_{out} refer to the direction of gas flow, whereas L_{in} and L_{out} refer to the direction of liquid flow. Gas and liquid come in contact in a counter current motion. Temperature undergoes a change throughout the tower (Figure 3 – left). Parameters such as temperature, pH and SO_2 removal efficiency are determined at certain heights of the tower denoted by cell *i* and *j* (Figure 3 – middle). The model is solved using an explicit finite difference method (4^{th}-order Runge-Kutta), where the output of the previous calculation step (e.g. cell *i*) is used as input to find the solution of the next step (e.g. cell *i* + 1) (Figure 3 – right). Corresponding equations as described in Eq. (8) to (27) were solved numerically with the schematic numerical model solution illustrated in Figure 3.

DOI: 10.5614/j.eng.technol.sci.2024.56.4.7

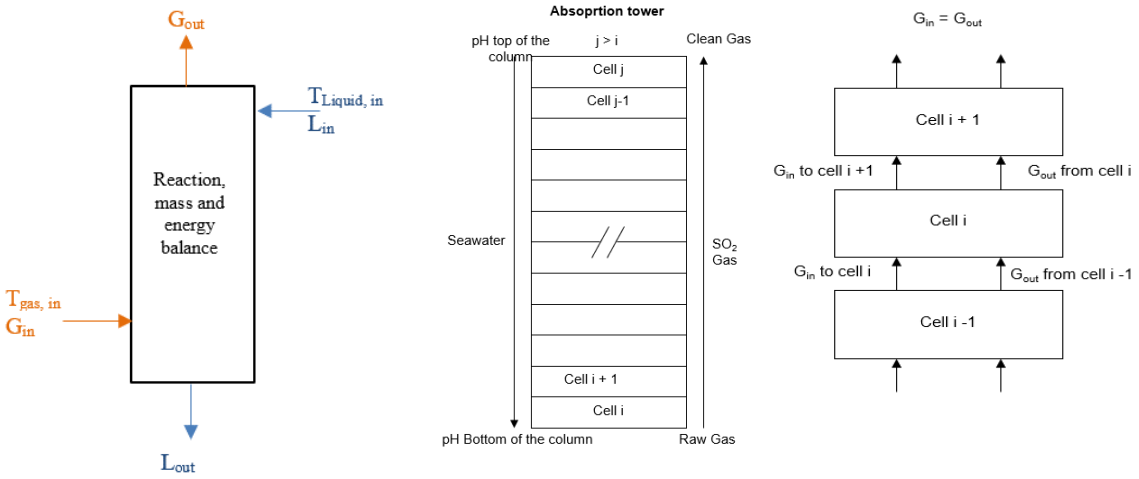

Figure 3 Schematic of numerical model solution in an absorption tower.

Results and Discussion

This study used field-scale data from an SWFGD absorber located in West Java, Indonesia. Model running was done by using a Henry's constant derived from said reference and additional information such as SWFGD dimension, flue gas temperature, seawater temperature, and both gas (1,691,277 Nm^3/h) and liquid (68,912 m^3/h) flowrate.

Chemical Species in Seawater

Table 2 shows the corresponding sulfur containing chemical species present in the seawater along the absorption tower. A general trend of the decrease of mole fraction of SO_2, SO_3^{2-}, SO_4^{2-}, HSO_3^- can be observed, as the distance from the bottom of the tower increases. On the other hand, an HSO_4^- increase can be observed, as the distance from bottom tower increases. If correlated with the corresponding pH, at a final pH of around 4.19, the seawater composition was dominated by HSO_3^-.

Table 2 Chemical species in seawater.

Distance form bottom tower (m)	Species concentration (mole/kg)				
	SO_2	SO_3^{2-}	SO_4^{2-}	HSO_3^-	HSO_4^-
0.00					
0.25	5.799668	0.157513	0.005485	155.0613	8.92E-06
2.75	5.527831	0.127626	0.005484	143.1394	9.28E-06
5.25	5.230671	0.115468	0.005484	130.5496	9.72E-06
7.75	4.903825	0.075943	0.005483	117.2456	1.03E-05
10.25	4.541677	0.051641	0.005483	103.1836	1.09E-05
12.75	4.136818	0.016279	0.005482	88.32917	1.18E-05
15.25	3.680244	5.20E-07	0.005481	72.70805	1.30E-05
17.75	3.149669	4.67E-07	0.005479	56.11986	1.48E-05
20.25	2.517221	4.54E-07	0.005476	38.66107	1.79E-05
22.75	1.666776	4.23E-07	0.005469	19.48326	2.52E-05
25.00	0.857215	4.17E-07	0.005450	6.426894	4.39E-05

Ph Value and Corresponding SO_2 Concentration in Gas Phase

Figure 4 shows the simulation result of the pH value along the absorption tower. By using an initial pH of 7.5, the final pH at the bottom of the tower was predicted to be 4.19. An abrupt decrease of pH at 22.75 m from the bottom of the tower was caused by the amount of SO_2 absorbed in the seawater, i.e., 5.79 mole/kg or 0.09 g/kg, close to the calculation result in [2].

Figures 5 and 6 show the removal efficiency of SO_2 concentration in the SWFGD absorber. Removal efficiency refers to the absorption of SO_2 from gas to liquid phase in seawater. At the farthest point from the bottom of the tower, removal efficiency reached 30.6% with a corresponding SO_2 concentration of 208.5 ppm. Comparison of data with the existing flue gas desulfurization absorber in an actual scale with the similar gas and liquid flowrate, the pH and initial SO_2 concentration resulted in a removal efficiency of 32.9% based on the SWFGD study in Indonesia.

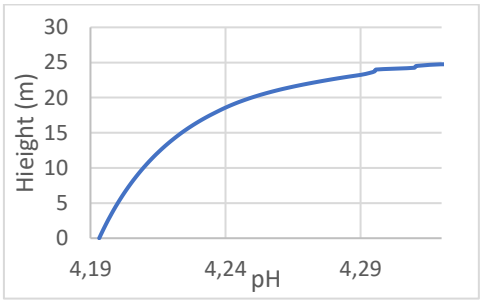

Figure 4 Value of pH along the absorption tower.

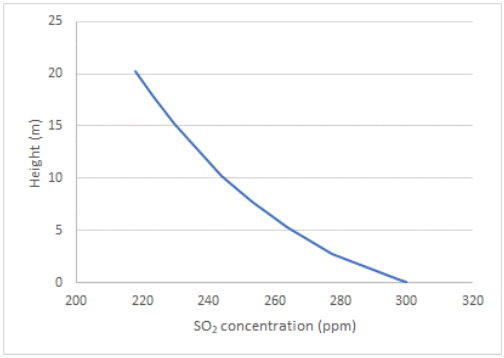

Figure 5 SO_2 concentration in the SWFGD absorber.

Figure 6 SO_2 removal efficiency in the SWFGD absorber.

Temperature

Figures 7 and 8 show the simulation result of the gas and liquid temperature along the counter current SWFGD absorber in the form of a percentage of the temperature decrease. As the mixing of the gas and liquid phase occurs simultaneously, it is obvious that the gas temperature will decrease from the bottom to the top of the tower (the gas is injected from the bottom of the tower), and the liquid temperature will increase from the top to the bottom of the tower (the liquid is injected from the top of the tower).

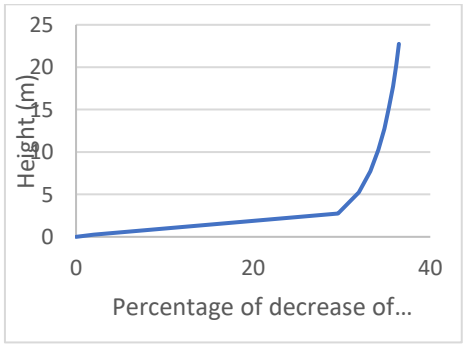

Figure 7 Percentage of decrease of the seawater temperature in the SWFGD absorber.

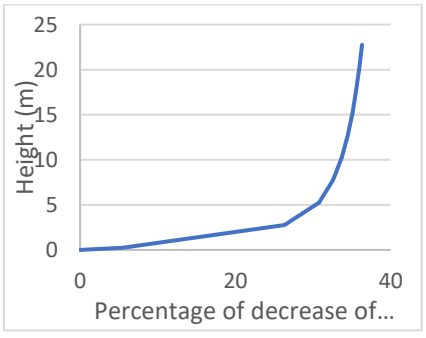

Figure 8 Percentage of decrease of the gas temperature in the SWFGD absorber.

DOI: 10.5614/j.eng.technol.sci.2024.56.4.7

Additional Model Testing (Mass Transfer Coefficient)

Table 3 shows the result of overall mass transfer coefficient testing with a k_l value of 0.083/s and 0.0415/s, respectively. With a lower overall mass transfer coefficient, a lower removal efficiency is produced. The result of overall mass transfer coefficient calibration is in accordance with the removal mechanism in a flue gas desulfurization absorber, where the increase of the overall mass transfer coefficient in the liquid phase will lead to a higher amount of SO_2 absorbed in the liquid. In this case, the decrease of the overall mass transfer coefficient in the liquid phase lowered the removal efficiency by 12.27% point. This value is very high relative to the initial removal efficiency.

Table 3 Overall mass transfer coefficient calibration (k_{l1} = 0.083 and k_{l2} = 0.0415).

Distance from bottom tower (m)	Concentration (fraction)		Efficiency (%)	
	k_{l1}	k_{l2}	k_{l1}	k_{l2}
0.00	0.000300	0.000299	0.000000	0.000000
0.25	0.000298	0.000297	0.760574	0.496849
2.75	0.000277	0.000285	7.509737	4.692743
5.25	0.000264	0.000277	12.1268	7.403493
7.75	0.000253	0.000271	15.6785	9.470021
10.25	0.000244	0.000266	18.63664	11.19566
12.75	0.000236	0.000261	21.19987	12.70009
15.25	0.00023	0.000257	23.47766	14.04719
17.75	0.000223	0.000254	25.53798	15.27565
20.25	0.000218	0.000250	27.42626	16.41100
22.75	0.000212	0.000247	29.17442	17.47101
25.00	0.000208	0.000245	30.64737	18.37134

Additional Model Testing (Laboratory-scale Experiments)

Due to limited field data, additional testing with laboratory-scale experiments was carried out to determine the model's validity. The parameters, i.e., packing details, salinity, pH, gas and liquid flowrate, L/G ratio and SO_2 concentration, were derived from [21] and were run using the same algorithm as previously presented. Figures 9 and 10 show the simulation results with SO_2 concentration being held constant at 500 ppm. The liquid flowrate was run at 40 L/h and 130 L/h, which corresponds to an L/G ratio of 1.06 kg/kg and 3.44 kg/kg, respectively. The developed model was found to be sensitive towards the increase of the L/G parameter with higher efficiencies present for a higher L/G value.

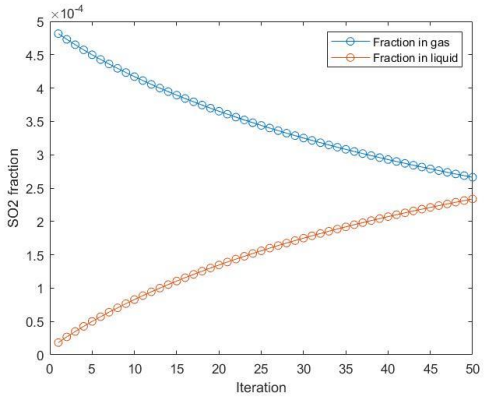

Figure 9 SO_2 fraction (initial SO_2 concentration = 500 ppm and L/G 1.06 kg/kg).

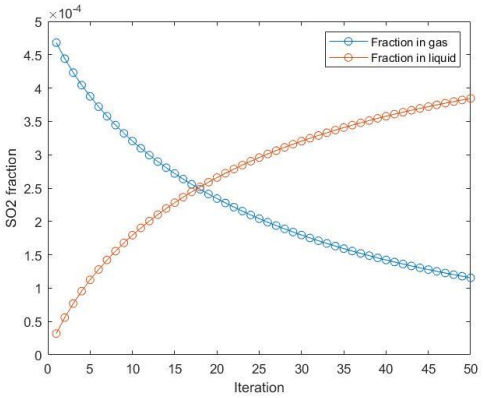

Figure 10 SO_2 fraction (initial SO_2 concentration = 500 ppm and L/G 3.44 kg/kg).

Moreover, the simulation results with the SO_2 concentration being held constant at 2,000 ppm (which corresponds to the highest concentration reported in [21]) produced a similar trend. Figures 11 and 12 show the simulation result with the SO_2 concentration being held constant at 2,000 ppm. The liquid flowrate was run at 40 L/h and 130 L/h, which corresponds to an L/G ratio of 1.06 kg/kg and 3.44 kg/kg, respectively. A reduction in

removal efficiency is to be expected, since the SO_2 concentration is increased with the L/G ratio being held constant. Table 4 summarizes a comparison between the SO_2 removal efficiency reported in [21] and the developed model.

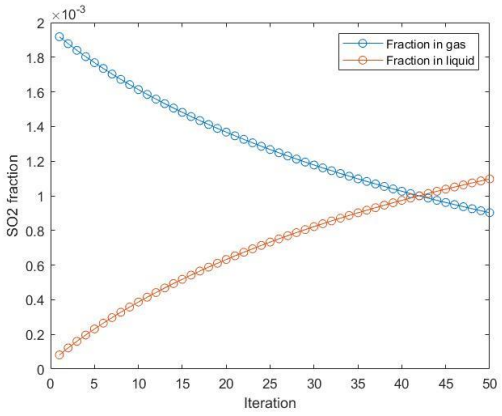

Figure 11 SO_2 fraction (initial SO_2 concentration = 2000 ppm and L/G 1.06 kg/kg).

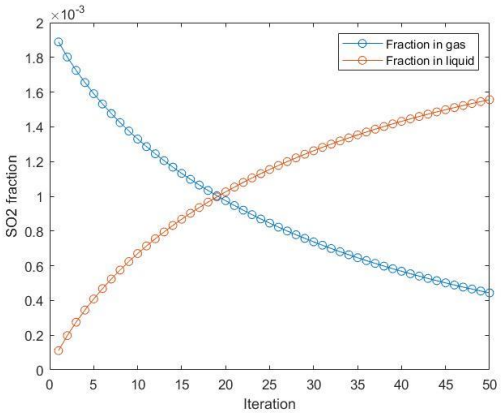

Figure 12 SO_2 fraction (initial SO_2 concentration = 2000 ppm and L/G 3.44 kg/kg).

Table 4 Comparison of SO_2 removal efficiency.

Parameter	Mass transfer coefficients (mole/m²s)		Efficiency (%)	
	Gas	Liquid	Model	Reference*
500 ppm				
L/G: 1.06 kg/kg	0.8	2.5	46.8	64
L/G: 3.44 kg/kg	1	1	76.9	90
2000 ppm				
L/G: 1.06 kg/kg	0.5	3	54.9	24
L/G: 3.44 kg/kg	0.8	4	77.8	72

*Reference is given as an estimate [21]

The discrepancies are likely caused by different assumptions of mass transfer coefficients used in the developed model. Additional running was done with a liquid and vapor mass transfer coefficient with a rate-based column of Sulzer MellaPak 250Y. The developed model showed adequate resemblance at a lower SO_2 concentration but overestimated the removal efficiency at a higher concentration. The model is able to show the general trend of SO_2 removal in an SWFGD, however refinement is needed to increase the model's accuracy. Although the developed model was proven to be sensitive towards variation of the liquid mass transfer coefficient (as shown in Table 3), further experimental-scale reactor testing is needed to validate the results.

Conclusion

Simulation of SO_2 absorption in an SWFGD absorber was carried out utilizing field data input from an existing SWFGD absorber in Indonesia. Calculation results showed that the developed model was able to illustrate that the changes in SO_2 concentration, pH as well as the removal efficiency along the absorption tower, were in accordance with the theory. The concentration distribution in SWFGD followed an exponential pattern, where a decrease of SO_2 gas with increasing tower height was observed. Temperature would decrease with an increase of SWFGD absorber height. However, some discrepancies were found due to the lack of information on several constants for the mass transfer of seawater absorbent. Differences in results can be overcome by validating the model with experimental-scale reactor testing.

Acknowledgement

This research was carried out with the help of funding from *Pengabdian kepada Masyarakat dan Inovasi* ITB (P3MI) ITB in 2019.

DOI: 10.5614/j.eng.technol.sci.2024.56.4.7

Compliance with ethics guidelines

The authors declare that they have no conflict of interest or financial conflicts to disclose.

This article does not contain any studies of human or animal subjects performed by any of the authors.

References

[1] Lamas, M.I., Rodríguez, C.G., Rodríguez, J.D. & Telmo, J., *Numerical Model of SO 2 Scrubbing with Seawater Applied to Marine Engines*, Polish Maritime Research, **23**, pp. 42-47, 2016. doi: 10.1515/pomr-2016-0019.

[2] Andreasen, A. & Mayer, S., *Use of Seawater Scrubbing for SO 2 Removal from Marine Engine Exhaust Gas*, Energy Fuels, **21**, pp. 3274-3279, 2007. doi: 10.1021/ef700359w.

[3] Oikawa, K., Yongsiri, C., Takeda, K. & Harimoto, T., *Seawater Flue Gas Desulfurization: Its Technical Implications and Performance Results,* Environ. Prog., **22**, pp. 67-73, 2003. doi: 10.1002/ep.670220118.

[4] Poullikkas, A., *Review of Design, Operating, and Financial Considerations in Flue Gas Desulfurization Systems*, Energy Technology & Policy, **2**, pp. 92-103, 2015. doi: 10.1080/23317000.2015.1064794.

[5] Głomba, M., *Technical Description of Parameters Influencing the pH Value of Suspension Absorbent Used in Flue Gas Desulfurization Systems*, Journal of the Air & Waste Management Association, **60**, pp. 1009-1016, 2010. doi: 10.3155/1047-3289.60.8.1009.

[6] Han, L., *Air Injection Techniques for Seawater Flue Gas Desulfurization (Swfgd) Aeration System*, p. 59.

[7] Darake, A.R., Hatamipour, M. & Hamzeloui, *SO_2 Removal by Seawater in a Packed–Bed Tower: Experimental Study and Mathematical Modeling,* Separation Science and Technology, **49**, 2014. doi: 10.1080/01496395.2013.872660.

[8] Oikawa, K. Yongsiri, C., Takeda, K. & Harimoto, T., *Seawater Flue Gas Desulfurization: Its Technical Implications and Performance Results*, Environ. Prog., **22**, pp. 67-73, 2003. doi: 10.1002/ep.670220118.

[9] Baaliña, A., Rodríguez, E., Santaballa, J.A. & Arce, A., *Prediction of the Acidity of Effluent from Fluegas Scrubbers using Seawater*, Environmental Technology, **18**, pp. 545-550, 1997. doi: 10.1080/09593331808616571.

[10] Rodríguez-Sevilla, J., Álvarez, M., Díaz, M.C. & Marrero, M.C., *Absorption Equilibria of Dilute SO 2 in Seawater*, J. Chem. Eng. Data, **49**, pp. 1710-1716, 2004. doi: 10.1021/je049833l.

[11] Roy, R.N., Roy, L.N., Vogel, K.M., Porter-Moore, C., Pearson, T., Good, C.E., Millero, F.J. & Campbell, D.M., *The Dissociation Constants of Carbonic Acid in Seawater at Salinities 5 to 45 and Temperatures 0 to 45°C*, Marine Chemistry, **44**, pp. 249-267, 1993. doi: 10.1016/0304-4203(93)90207-5.

[12] UNEP/GEC Session, *Reuse of Seawater for Flue Gas Desulfurization –Its Practical Information from an Engineering Point of View*, FGD Project Headquarters Fujikasui Engineering Co., Ltd. Accessed: http://gec.jp/gec/en/Activities/th05-presen3.pdf (Mar. 28, 2022)

[13] *Temperature Dependence of the pH of pure Water - Chemistry LibreTexts*, Accessed: https://chem.libretexts.org/Bookshelves/Physical_and_Theoretical_Chemistry_Textbook_Maps/Supplemental_Modules_(Physical_and_Theoretical_Chemistry)/Acids_and_Bases/Acids_and_Bases_in_Aqueous_Solutions/The_pH_Scale/Temperature_Dependence_of_the_pH_of_pure_Water (Mar. 28, 2022)

[14] Baaliña, A., Rodriguez, E., Santaballa, J.A. & Arce, A., *Acidity of Effluent from Inert Gas Systems Using Seawater Scrubbing*, Environmental Technology, **17**, pp. 331-335, 1996. doi: 10.1080/09593331708616392.

[15] Hocking, M.B. & Lee, G.W., *Calculated Sulfur Dioxide Equilibria at Low Concentrations between Air and Water*, Water Air Soil Pollut, **8**, pp. 255-262, 1977. doi: 10.1007/BF00541911.

[16] Treybal, R.E., *Mass Transfer Operations*. Singapore: McGraw-Hill, 1981.

[17] Piché, S., Lévesque, S., Grandjean, B.P.A. & Larachi, F., *Prediction of HETP for Randomly Packed Towers Operation: Integration of Aqueous and Non-Aqueous Mass Transfer Characteristics into One Consistent Correlation*, Separation and Purification Technology, **33**, pp. 145-162, 2003. doi: 10.1016/S1383-5866(03)00005-4.

[18] Nevers, N.D., *Air Pollution Control Engineering*, Second. McGraw-Hill International Editions.

[19] Sander, R., *Compilation of Henry's Law Constants for Inorganic and Organic Species of Potential Importance in Environmental Chemistry*, p. 107.

[20] Sawyer, C.N., *Chemistry for Environmental Engineering and Science*. McGraw-Hill, 2003.

[21] Flagiello, D., Erto, A., Lancia, A. & Di Natale, F., *Experimental and Modelling Analysis of Seawater Scrubbers for Sulfur Dioxide Removal from Flue-gas*, Fuel, **214**, pp. 254-263, 2018. doi: 10.1016/j.fuel.2017.10.098.
.

Manuscript Received: 5 January 2024
Revised Manuscript Received: 16 May 2024
Accepted Manuscript: 16 May 2024